Solution-processed nickel tetrabenzoporphyrin thin-film transistors

Patrick B. Shea and Jerzy Kanicki[a)]
Organic and Molecular Electronics Laboratory, Department of Electrical Engineering and Computer Science, The University of Michigan, Ann Arbor, Michigan 48109

Lisa R. Pattison and Pierre Petroff
Department of Materials Science and Engineering, The University of California, Santa Barbara, California 93106

Manami Kawano, Hiroko Yamada, and Noboru Ono
Department of Chemistry in the Faculty of Science, Ehime University, Bunkyo-cho 2-5, Matsuyama 790-8577, Japan

(Received 17 February 2006; accepted 25 May 2006; published online 2 August 2006)

We describe nickel tetrabenzoporphyrin (NiTBP) as a solution-processible organic semiconductor. Whereas porphyrins in an unmodified state are typically planar and insoluble, a precursor synthetic route (NiCP) was used to deposit thin films via solution. Amorphous, insulating thin films of NiCP were deposited, and thermally converted to polycrystalline, semiconducting NiTBP. Films were studied using optical absorption and microscopy, atomic force microscopy, and x-ray diffraction. Highly concentrated NiCP was shown to form large, needle-shaped crystals drop-cast from solution. NiTBP thin-film field-effect transistors fabricated from spun-cast films demonstrated charge-carrier field-effect mobilities on the order of 0.1 and 0.2 $cm^2/V\ s$ and accumulation threshold voltages of −19 and −13, in the linear and saturation regimes, respectively. © *2006 American Institute of Physics*. [DOI: 10.1063/1.2220641]

I. INTRODUCTION

Organic field-effect transistors (OFETs) can be fabricated using a wide variety of organic semiconductors. Among them, metallophthalocyanine (MPc) thin films have demonstrated high electronic performance in terms of field-effect mobility (μ_{FE}), ON-/OFF-current ratio (I_{ON}/I_{OFF}), and subthreshold slope (S).[1,2] Copper phthalocyanine (CuPC) in particular is well studied and has demonstrated μ_{FE} exceeding 1 $cm^2/V\ s$.[3–5] Nickel phthalocyanine (NiPC), on the other hand, typically demonstrates μ_{FE} lower than that of CuPC by several orders of magnitude.[6–9] Furthermore, most work on MPc OFETs has focused on thin films deposited using evaporation deposition methods, thus apparently precluding the large-area, low-cost processing hypothetically afforded by solution deposition.

Much organic transistor research has focused on the development of soluble precursor forms of small molecules, especially pentacene.[10–15] Typically the small molecule is functionalized using a bulky, unstable side chain that, following thin-film deposition, can easily be removed by a thermal or optical process. Solution-processed OFETs have been fabricated utilizing tetrabenzoporphyrin (TBP),[16–19] an organic small molecule similar to phthalocyanine that can be synthesized in a soluble precursor form[20,21] with a variety of configurations for the core atoms.[22,23] By varying the core atoms with only a minimal change in the chemical synthesis, the properties of the porphyrin can be tailored to a desired application. In organic transistors, incorporation of a metal into the TBP molecule might serve to enhance charge mobility, as well as alter optical absorption or chemical sensitivity. Furthermore, much as different MPcs were explored for OFET use, it is worthwhile to examine whether MTBP films respond similarly. In this work we report the use of solution-processed nickel tetrabenzoporphyrin (NiTBP) for transistor applications, and provide several different experimental characterizations of solution-processed NiTBP films. By substituting nickel into the core of the TBP molecule, millimeter-scale crystallization and high conductivity were observed for thermally annealed, spun-cast thin films.

II. FILM PREPARATION

Synthesis of the soluble precursors used here has been described elsewhere.[20–22] In all studies, precursor solutions of nickel tetrabicycloporphyrin in chloroform (NiCP, 0.9 wt%) were utilized (Fig. 1). Prior to solution deposition, all substrates were washed with acetone and isopropyl alcohol, exposed to ultraviolet light and ozone for 20 min, and soaked in 200 proof ethanol for 20 min. All films were processed in the N_2 atmosphere of a glove box. Drop-cast films were formed by dropping NiCP onto the substrate and allowing the solvent to evaporate at room temperature, without control of the final film thickness. Spun-cast film thickness

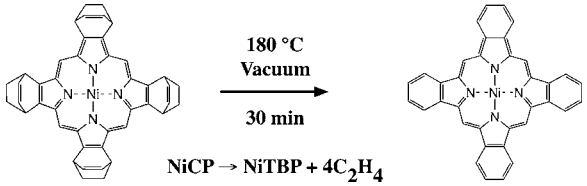

FIG. 1. Molecular structure of the precursor, NiCP, and the thermally annealed semiconductor, NiTBP.

[a)]Electronic mail: kanicki@eecs.umich.edu; URL: http://www.eecs.umich.edu/omelab

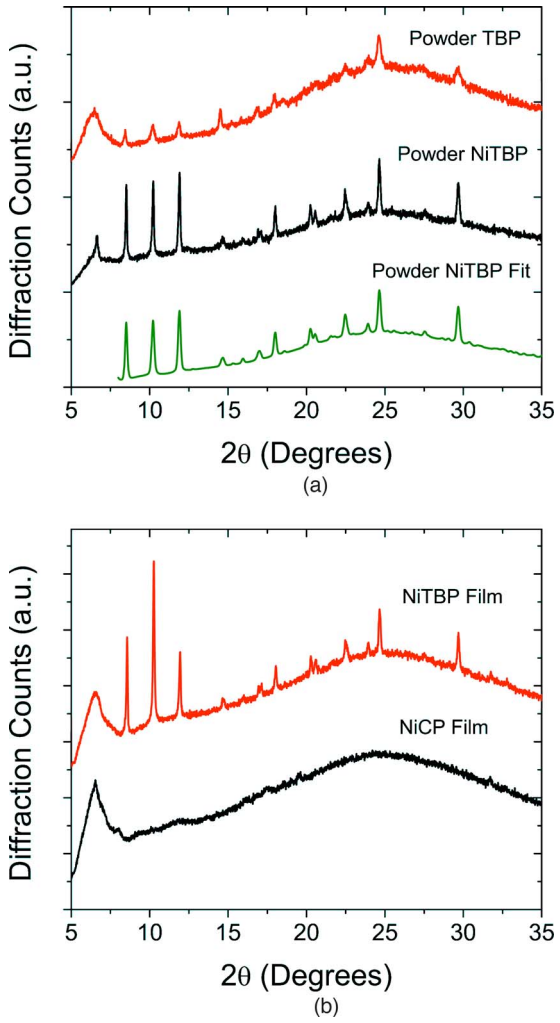

FIG. 2. (Color online) XRD spectra for NiTBP and NiCP powders and thin films.

varied between 100 and 250 nm, depending on spinning speed. Following solution deposition, samples were converted to NiTBP by baking at 180 °C for 30 min under vacuum (Fig. 1).

III. MICROSTRUCURAL DIFFRACTION

Thin films on bare crystalline silicon (c-Si) substrates (n-type, 100 Ωcm, ⟨100⟩) were used for x-ray diffraction (XRD) measurements. Powder-mode XRD in reflection geometry was performed with a Philips XPERT MPD diffractometer with Cu$K\alpha$ radiation (40 kV/30 mA) over $4° \leq 2\theta \leq 35°$. XRD analysis on NiTBP and TBP powder was also performed by thermally converting NiCP and CP powder to NiTBP and TBP using the same thermal annealing process as for solution-cast films. All XRD measurements were performed under vacuum.

XRD patterns for drop-cast NiCP and NiTBP thin films, and TBP and NiTBP powder, are shown in Fig. 2. The pattern for drop-cast NiCP displays no measurable peaks and exhibits the broad hump characteristic of thin films. Upon thermal annealing, numerous diffraction peaks indicative of the formation of crystal planes appear, but because the film retains some of its random nature, the broad hump is still present. Drop-cast NiTBP thin films display the same diffraction peaks as powder NiTBP, and in both spectra low- and high-angle 2θ reflections have large intensities. Table I summarizes the 2θ peaks from Fig. 2 for powder NiTBP and TBP. While the intensities of each spectrum are not directly comparable, we can make several conclusions based on the XRD spectra. NiTBP powder and thin-film diffraction peaks display a significantly larger relative intensity compared to their background, indicating large crystalline volumes present in the film. Many NiTBP 2θ diffraction peaks over the entire 2θ range display large areal intensities, indicating that the average XRD spectrum of the NiTBP film displays no preferred crystal orientation. On the other hand, preliminary low grazing angle XRD spectra display variation in 2θ peak intensity with grazing angle, which indicates a variation in crystal orientation with NiTBP film thickness. Further evidence of crystal orientation variation with film thickness is provided during atomic force microscopy (AFM) analysis.

TABLE I. Comparison of diffraction peaks for TBP and NiTBP powder from Fig. 2, with the corresponding Miller indices.

TBP	*NiTBP*	(*hkl*)
8.43	8.51	$10\bar{1}$
10.21	10.22	101
11.87	11.90	002
14.49	14.64	$20\bar{1}$
16.95	16.92	$1\bar{1}1$
17.98	18.01	012
20.66	20.25	112
22.47	22.45	013
24.62	24.65	113
29.70	29.67	022

XRD spectra from both drop-cast and powder NiTBP (Fig. 2) were used to define the NiTBP unit cell via the Pawley and Rietveld powder refinement methods combined with Pareto optimization to both match the experimental XRD spectra and minimize the potential energy.[24–26] The 2θ positions of the diffraction peaks between TBP and NiTBP indicate a similar crystallographic structure, namely that the unit cell is monoclinic with $P2_1/n$ symmetry. Fitting the XRD powder data produces a unit cell with lattice dimensions of $a=1.236$ nm, $b=0.6578$ nm, $c=1.519$ nm, and $\beta=100.62°$. The simulated XRD spectrum based on this fit is included in Fig. 2(a), and the molecular structure of the NiTBP unit cell is shown in Fig. 3. The Miller indices for the NiTBP 2θ reflections are also shown in Table I. Additionally, preliminary geometry optimization computations indicate slight nonplanarity in the individual NiTBP molecules (Fig. 3), and agree with the bond angles and lengths reported for other nickel porphyrin molecules.[27–34]

IV. OPTICAL ABSORBANCE AND ATOMIC FORCE MICROSCOPY

Quartz substrates and a Varian-Cary 500 UV-visible (UV-vis) spectrometer were used for optical absorbance measurements. Absorbance versus wavelength was measured in

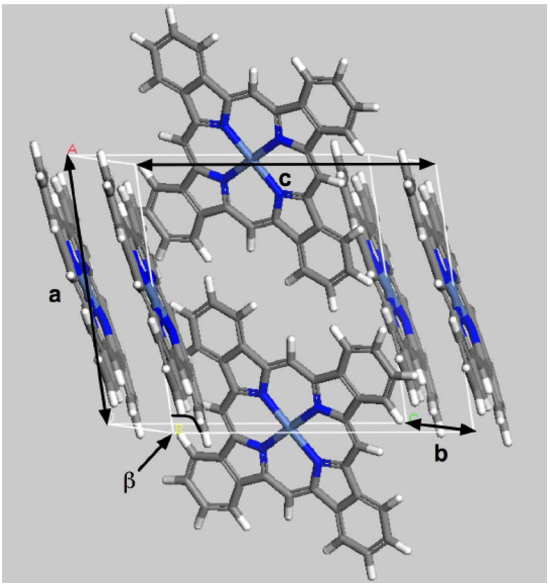

FIG. 3. (Color online) Proposed molecular structure of the monoclinic NiTBP unit cell.

air at room temperature immediately following thin-film thermal conversion over a photon wavelength (λ) range of $200 \leq \lambda$ (nm) ≤ 500.

AFM was performed using a Digital Instruments Multi-Mode NanoScope in tapping mode, with films being cast onto $n++$ c-Si substrates coated with a 100-nm-thick thermal oxide layer.

Many studies have examined the optical properties of free-base and metal-substituted porphyrin-based macromolecules, typically suspended in solution or in a gaseous phase.[22,32,35–39] Typical absorption spectra of porphyrin molecules include a Soret, or B, band (a strong optical absorption band in the near-UV range in a heme or heme-like molecule) around $h\nu = 3$ eV and Q bands (weaker optical absorption bands in the visible range) between $1.75 < h\nu$ (eV) < 2.75,[37] with variations in peak position and peak splitting due to metal incorporation and the peripheral substituents (here, Ni and benzene, respectively). The solid NiTBP and NiCP films presented here display these typical optical properties; absorbance spectra for drop- and spun-cast NiTBP and spun-cast NiCP are displayed in Fig. 4. For

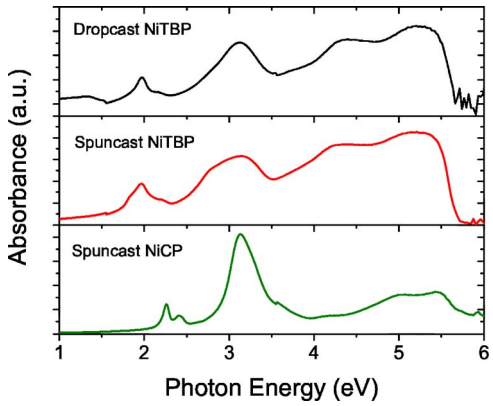

FIG. 4. (Color online) Optical absorbance spectra for drop- and spun-cast NiTBP, and spun-cast NiCP thin films.

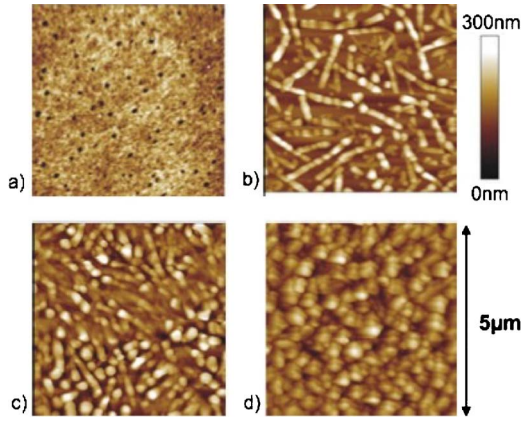

FIG. 5. (Color online) Tapping-mode AFM height images of NiCP and NiTBP spun cast onto SiO_2 surfaces. For image (a), the height scale is 7 nm, for (b)–(d) the scale is 300 nm. All images scan 5×5 μm^2 areas. (a) NiCP precursor; (b) after thermal conversion, NiTBP in the thin region of film showing the morphology at the interface; (c) The thicker region of the NiTBP film, showing the disordered piling of rods; (d) an image on the surface of a thick NiTBP crystallite.

both NiTBP films the maximum occurs at a photon energy of 5.2 eV, and for NiCP the maximum occurs at a photon energy of 3.1 eV. The NiTBP spectra display three large, broad absorption peaks at 2.0, 3.1, and 5.2 eV, a prominent shoulder at 4.4 eV, and a quickly declining absorbance above 5.5 eV. The spun-cast NiCP spectrum displays absorbance peaks at 2.3, 2.4, 3.1, and 5.4 eV. The shift of absorption peaks at 2.3 and 2.4 eV in NiCP to 2.0 eV in NiTBP may indicate a shift in the π-π^* transition during thermal conversion. Comparatively, in solid films of NiPC the π-π^* transition occurred at a photon energy around 1.8 eV and was attributed to a ligand-centered transition.[40] Also of note in Fig. 4 are the similarities between the absorption spectra of both NiTBP films. Because of their similar absorption, and therefore their electronic structure, drop-cast and spun-cast NiTBP films likely form similar crystal structures upon thermal annealing. Absorption of NiCP needles was also studied, and found to be equivalent to the spectrum of the spun-cast NiCP films. The presence of a broad absorption spectrum, such as for NiTBP, indicates the formation of wide energy bands near the band gap with many possible transitions, typical of highly ordered materials, whereas less ordered NiCP displays sharp peaks and a less broad optical absorbance, indicating fewer transitions.[41–43]

AFM height micrographs of spun-cast NiCP and NiTBP are shown in Fig. 5. Before thermal annealing, NiCP thin films are amorphous and smooth, with an average surface roughness of 5 nm [Fig. 5(a)]. For the thinnest regions [Fig. 5(b)], rod formation is observed on the gate insulator surface, with an average rod height and width of 110 and 200 nm, respectively, and lengths up to 2 μm. AFM also indicates that the rods tend to grow with their long axes parallel to the plane of the surface or at moderate angles of $8° - 15°$ with respect to the surface plane. AFM on thicker NiTBP films [Fig. 5(d)] indicates that out-of-plane orientation of NiTBP needles occurs away from the insulator surface, with aggregates piled on top of each other with random orientation. Hence, NiTBP rod orientation is expected to display a depen-

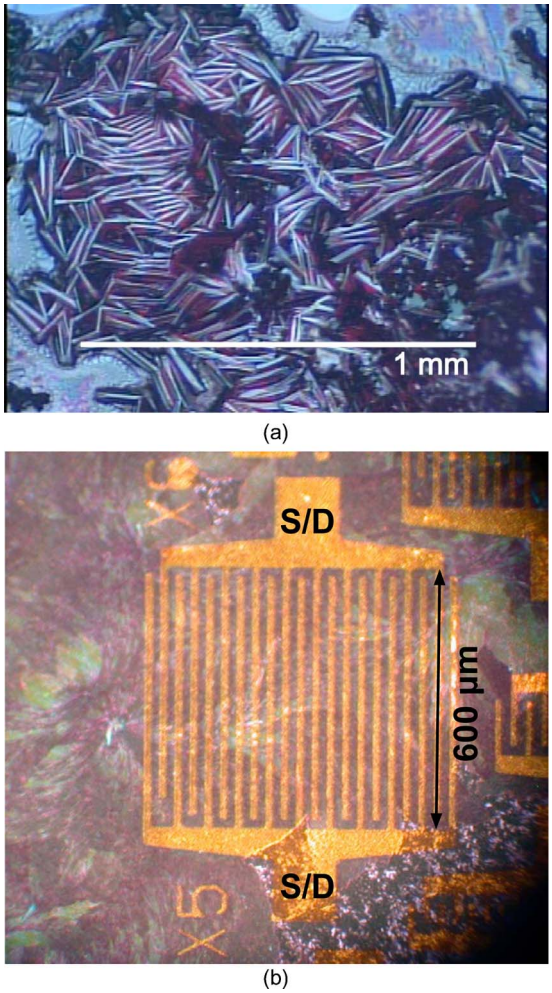

FIG. 6. (Color online) Optical micrographs of drop- and spun-cast NiTBP thin films.

dence on film thickness. Close to the gate insulator surface, or when there is a low density of molecules, NiTBP rods align parallel, or nearly so, to the interface. As the density increases, the NiTBP rods gradually begin to tilt with their long axis at an angle from the gate insulator surface, which in Fig. 5(c) is noted by the more pronounced height at the ends of the rods. At a critical rod density and distance from the gate insulator surface, NiTBP rod formation occurs with random orientation, leading to a rough surface in thicker films. From these observations we can conclude that the rod, and crystal, orientation changes with the film thickness and more ordered orientation is observed near the NiTBP-gate insulator interface.

V. SPUN-CAST THIN-FILM TRANSISTORS

Optical micrographs of drop- and spun-cast films on thermally oxidized *c*-Si are shown in Figs. 6(a) and 6(b), respectively. As expected, drop casting led to several different regions of crystallization, varying with the film thickness, whereas spin casting produced uniform thin films. During drop deposition, as the solvent evaporated, striae were observed indicating variations in the film thickness, until the large, needle-shaped crystallites formed [Fig. 6(a)]. Following thermal annealing, three types of crystal domains were observed: widely dispersed, small (≈ 1 μm in length) needles occurring where the film was invisible to the naked eye or to UV-vis spectroscopy, but discernable by AFM [Fig. 5(b)]; a thin-film regime [Fig. 6(b)] observable by UV-vis and with crystallization as in the spun-cast films studied by AFM (Fig. 5) and used for OFETs; and a thick regime [Fig. 6(a)], typically about 1 mm thick, where large needles formed but adhered poorly to substrates such as silicon nitride and silicon oxide.

OFETs and four-probe structures were fabricated utilizing n++ *c*-Si substrates coated with a 100-nm-thick thermal SiO_2 layer to serve as the unpatterned gate electrode and gate insulator dielectric, respectively. The areal gate capacitance was measured to be $C_i = 24.5$ nF/cm^2. Following thermal annealing of a spun-cast thin film, Au (60 nm) was thermally evaporated through a stencil mask to form the source and drain electrodes in a staggered configuration.[44] Devices were tested in the dark and in air using a Hewlett-Packard 4156A semiconductor parameter analyzer. Before electrical testing, OFETs were isolated by scratching away a ring of the semiconductor thin film around the device. The measured gate current (I_G) was negligible compared to the drain current (I_D). NiTBP behaves as a p-type semiconductor, and so to operate OFETs as accumulation devices, the accumulation threshold voltage (V_T) is negative relative to ground, as are the typical operating gate-to-source and drain-to-source biases (V_{GS} and V_{DS}, respectively). The source electrode was set as ground. Thus, the device is in the ON state when $V_{GS} < V_T$, and in the OFF state when $V_{GS} > V_T$. For transfer characteristics (I_D vs V_{GS}), V_{GS} was swept from the ON state to the OFF state; for output characteristics (I_D vs V_{DS}), V_{GS} was stepped from the ON state to the OFF state, and during each step V_{DS} was swept from 0 V into saturation ($V_{DS} \ll V_{GS} - V_T$). Electrical contact to the gate electrode was made with an indium gallium eutectic to the substrate backside. For further study on OFET operation, we refer the reader to several comprehensive reviews.[10,44–47]

Attempts were made to fabricate NiTBP OFETs by drop-casting NiCP onto substrates with coplanar source and drain electrodes.[44] Large needle-shaped crystals formed but displayed no transistor behavior before or after thermal annealing. The absorption spectra for drop- and spun-cast films (Fig. 4) indicate very similar electronic structures, such that transistors might also be made from the needle-shaped crystals. However, in our tests the drop-cast crystals adhered poorly to the substrate and source and drain electrodes, preventing electrical contact between two coplanar electrodes. In the future, it may be possible to improve NiCP crystal adhesion to the substrate using a dielectric surface modification, or to the source and drain electrodes using conformal, conducting polymer electrodes such as PEDOT[48] instead of rigid metal electrodes.

The electrical measurements presented here are for a single device with channel width (W) of 2080 μm and a channel length (L) of 100 μm. OFET electrical performance with respect to μ_{FE} and V_T was found to vary within ±25% for different runs across all functional devices, with no consistent trend due to device geometry, including channel length and width. Output characteristics are shown in Fig.

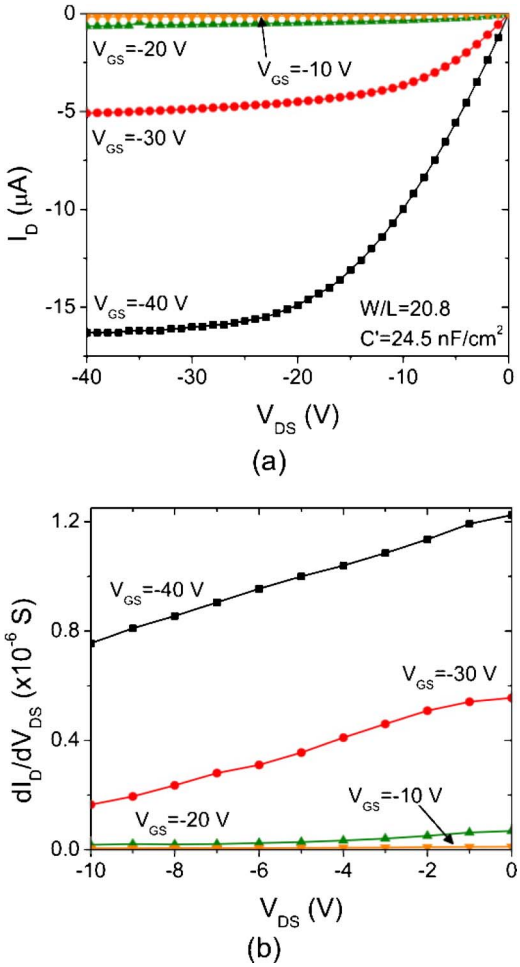

FIG. 7. (Color online) Output and conductance characteristics for an NiTBP OFET.

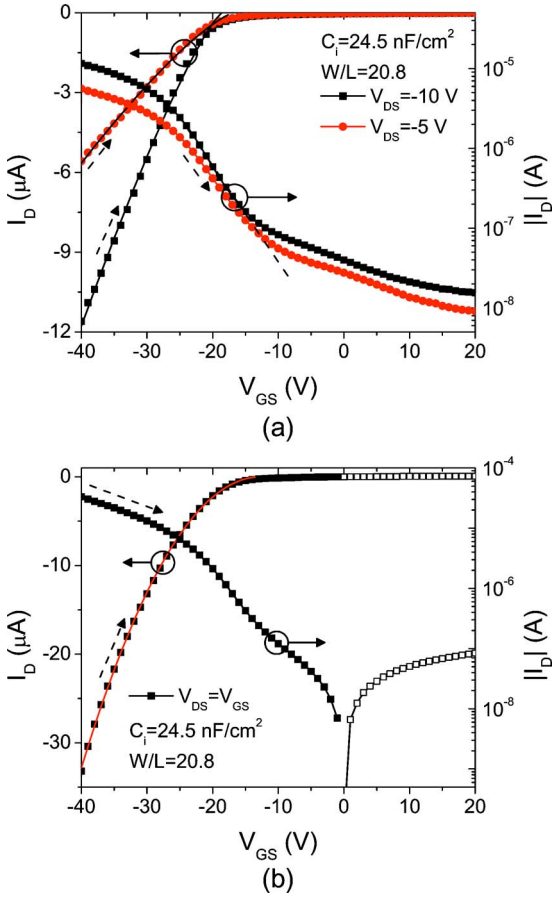

FIG. 8. (Color online) Transfer characteristics for an NiTBP OFET.

7(a). The output characteristics exhibit distinct linear and saturation regimes, with the channel conductance $g_d = dI_D/dV_{DS}$ approaching zero in saturation [Fig. 7(b)]. The channel conductance decreases monotonically with V_{DS}, indicating ohmic source and drain electrode behavior. Furthermore, near $V_{DS}=0$ V, minimal offset, on the order of 1 nA, is observed in I_D, indicating that gate and film leakage are negligible. Transfer characteristics in the linear regime ($V_{DS}=-10$ and -5 V) and saturation regime($V_{DS}=V_{GS}$) are shown in Fig. 8 on both a linear and semilogarithmic scale. A nonlinear FET current-voltage relationship has been previously developed that accounts for dispersive charge transport resulting in a V_{GS}-dependent μ_{FE}.[19,49–51] This methodology was used to extract the NiTBP OFET electrical parameters, and in the linear regime ($|V_{DX}| < |V_{GS}-V_T|$), I_D is expressed by

$$I_D^{\mathrm{lin}} = -\frac{W}{L}\mu_{\mathrm{FE0}}^{\mathrm{lin}} C_i (V_{GS} - V_T^{\mathrm{lin}})^{\gamma} V_{DS}, \tag{1}$$

where $\mu_{\mathrm{FE0}}^{\mathrm{lin}}$ is a prefactor constant for the mobility with units of $\mathrm{cm}^{\gamma}/\mathrm{V\,s}$. Field-effect mobility is then given by a V_{GS}-dependent relation

$$\mu_{\mathrm{FE}}^{\mathrm{lin}}(V_{GS}) = \mu_{\mathrm{FE0}}^{\mathrm{lin}}(V_{GS} - V_T^{\mathrm{lin}})^{\gamma-1}. \tag{2}$$

In the linear regime, $V_{DS}=-10$ V; fitting Eq. (1), we find $V_T^{\mathrm{lin}}=-18.9$ V, $\gamma=1.2$, and $\mu_{\mathrm{FE}}^{\mathrm{lin}}=0.13\ \mathrm{cm}^2/\mathrm{V\,s}$ at $V_{GS}=-40$ V. Similarly, in the saturation regime ($|V_{DS}| > |V_{GS}-V_T|$), I_D is expressed by

$$I_D^{\mathrm{sat}} = -\frac{W}{(\gamma+1)L}\mu_{\mathrm{FE0}}^{\mathrm{sat}} C_i (V_{GS} - V_T^{\mathrm{sat}})^{\gamma+1}, \tag{3}$$

with the saturation field-effect mobility being similarly defined as in Eq. (2) by

$$\mu_{\mathrm{FE}}^{\mathrm{sat}}(V_{GS}) = \mu_{\mathrm{FE0}}^{\mathrm{sat}}(V_{GS} - V_T^{\mathrm{sat}})^{\gamma-1}. \tag{4}$$

In the saturation regime we set $V_{DS}=V_{GS}$ and find $V_T^{\mathrm{sat}}=-13.0$ V, $\gamma=1.1$, and $\mu_{\mathrm{FE}}^{\mathrm{sat}}=0.22\ \mathrm{cm}^2/\mathrm{V\,s}$ at $V_{GS}=-40$ V. However, as displayed in Fig. 8, in the linear regime an ON-/OFF-current ratio of, at most, 10^3 has been measured, which is two orders of magnitude less than for free-base TBP.[19] A low ON-/OFF-current ratio is also prevalent in the saturation regime, with a best-case ratio approaching 10^3 between $V_{GS}=-40$ V and $V_{GS}=0$ V. The higher bulk conductivity, as compared to free-base TBP, manifests itself in the saturation regime as a small, positive I_D for $V_{GS}>0$ V. This conductivity may also produce the large subthreshold slope, 7.4 V/dec, in that the large I_D in the OFF state produces a gradual transition from ON to OFF. The large subthreshold slope could also be an indication of a significant trap states density resulting from the random orientation of NiTBP

growth near the film's top surface, leading to a back-channel effect. The subthreshold slope can be related to the apparent densities of trap states, either in the surface trap states, N_{ss} (cm^{-2} eV^{-1}), or the bulk trap states, N_{bs} (cm^{-3} eV^{-1}), as calculated by[52]

$$S = \frac{kT}{q \log(e)}[1 + C_i(\sqrt{\epsilon_s N_{bs}} + qN_{ss})], \tag{5}$$

where k is Boltzmann's constant, T is the temperature, q is the electronic charge, and ϵ_s is the semiconductor permittivity. The dielectric constant of solid NiTBP is at this time unknown, but if we assume $N_{bs} \ll N_{ss}$, the maximum N_{ss} approaches 1.88×10^{13} cm^{-2} eV^{-1}, whereas in pristine TBP $N_{ss}^{\max} = 2.9 \times 10^{12}$ cm^{-2} eV^{-1}.[19]

Thin-film resistivity was examined using a four-probe structure.[53] By forcing a current (I) from 0 to −1 nA through the two outer electrodes, a potential (ΔV) is induced between two inner electrodes. The quotient of ΔV and I is related to the film resistivity, ρ (Ω cm), by

$$\rho = \frac{\Delta V}{I} \frac{W^* t_{\text{film}}}{L'}, \tag{6}$$

where W^* is the width of the electrodes (1500 μm), t_{film} is the semiconductor film thickness (150 nm), and L' is the inter-electrode spacing (20 μm). The resulting resistivity for NiTBP is on the order of 7×10^3 Ω cm. Furthermore, in OFET measurements I_{OFF} displays a distinct dependence on V_{GS} that does not result from a significant I_G leakage current. Having determined the resistivity via the four-probe method, we can relate this to the expected OFF-state I_D in an OFET by

$$I_D = \frac{V_{DS} x_j W}{\rho L}, \tag{7}$$

where x_j is the charge conduction (or channel layer) thickness. The charge conduction thickness can vary significantly, from on the order of 5–10 nm in strong accumulation[54] to the thin-film thickness in the OFF state. For NiTBP, using $W = 2080$ μm, $L = 100$ μm, $V_{DS} = -10$ V, and $x_j = 100$ nm, I_D is expected to be approximately −200 nA, which corresponds approximately to the measured I_D near $V_{GS} = -15$ V in Fig. 8(a).

Several rationales were considered to explain the high thin-film conductivity. Elemental analysis did not reveal an excess of free Ni impurities in the precursor powders (7.7% measured versus 8.6% ideal, by weight). It has been reported that nickel porphyrins have similar band gaps to metal-free porphyrins,[33] which would indicate that the highest occupied molecular orbital (HOMO) level for NiTBP is around 2.9 eV and the lowest unoccupied molecular orbital (LUMO) level is around 5.1 eV.[55] Based on the large value of the subthreshold slope, it is likely that NiTBP thin films have a high density of trap states localized within the grain boundaries. This was confirmed by measuring the change in the film conductivity during exposure to broadband illumination.[56,57] It was found that light exposure had a minimal effect on I_D in the ON state for NiTBP and TBP OFETs; the light-to-dark I_D ratio in the OFF state for NiTBP is slightly less than one order of magnitude, whereas for TBP the ratio exceeds two orders of magnitude, indicating that NiTBP has a higher density of grain boundary trap states (recombination centers). While NiTBP displays significantly larger crystals than TBP, an increased grain boundary trap states density could result from the random NiTBP rod orientation that occurs with increasing film density for thicker films. The large subthreshold slope, and high overall conductivity, could also simply be a result of the incorporation of the Ni atom into the TBP molecule, assuming that Ni atoms will participate in charge carrier conduction, as has been shown in iodine-oxidized (tetrabenzoporphyrinato)nickel(II) and in one-dimensional simulations of NiTBP.[58,59]

VI. CONCLUSIONS

We have demonstrated solution-processible nickel tetrabenzoporphyrin as the active material in organic thin-film FETs. These devices demonstrated field-effect mobilities around 0.2 cm^2/V s, indeed one of the highest field-effect mobilities to date for solution-processed organic transistors. Optical absorbance measurements displayed similar absorbance spectra to previous studies on metallotetrabenzoporphyrin molecules. XRD indicated the formation of crystal planes during thermal annealing, with AFM showing a flat, amorphous film converting to a rough, polycrystalline thin film. Four-probe conductivity measurements revealed that nickel tetrabenzoporphyrin thin films had a low resistivity. The crystal structure of solid NiTBP processed from solution was presented.

[1] R. W. I. de Boer, A. F. Stassen, M. F. Craciun, C. L. Mulder, A. Molinari, S. Rogge, and A. F. Morpurgo, Appl. Phys. Lett. **86**, 262109 (2005).
[2] J. Zhang, H. Wang, X. J. Yan, J. Wang, J. W. Shi, and D. H. Yan, Adv. Mater. (Weinheim, Ger.) **17**, 1191 (2005).
[3] Z. Bao, A. J. Lovinger, and A. Dodabalapur, Appl. Phys. Lett. **69**, 3066 (1996).
[4] K. Xiao, Y. Q. Liu, G. Yu, and D. B. Zhu, Synth. Met. **137**, 991 (2003).
[5] R. Zeis, T. Siegrist, and C. Kloc, Appl. Phys. Lett. **86**, 022103 (2005).
[6] G. Guillaud, R. Madru, M. A. Sadoun, and M. Maitrot, J. Appl. Phys. **66**, 4554 (1989).
[7] G. Guillaud, R. B. Chaabane, C. Jouve, and M. Gamoudi, Thin Solid Films **258**, 279 (1995).
[8] R. B. Chaabane, A. Ltaief, C. Dridi, H. Rahmouni, A. Bouazizi, and H. B. Ouada, Thin Solid Films **427**, 371 (2003).
[9] C. Clarisse, M. Riou, M. Gauneau, and M. Le Contellec, Electron. Lett. **24**, 674 (1988).
[10] A. R. Brown, C. P. Jarrett, D. M. de Leeuw, and M. Matters, Synth. Met. **88**, 37 (1997).
[11] A. R. Brown, A. Pomp, D. M. de Leeuw, D. B. M. Klaasen, and E. E. Havinga, J. Appl. Phys. **79**, 2136 (1996).
[12] P. T. Herwig and K. Müllen, Adv. Mater. (Weinheim, Ger.) **11**, 480 (1999).
[13] A. Afzali, C. D. Dimitrakopoulos, and T. L. Breen, J. Am. Chem. Soc. **124**, 8812 (2002).
[14] A. Afzali, C. D. Dimitrakopoulos, and T. O. Graham, Adv. Mater. (Weinheim, Ger.) **15**, 2066 (2003).
[15] M. M. Payne, J. H. Delcamp, S. R. Parkin, and J. E. Anthony, Org. Lett. **6**, 1609 (2004).
[16] S. Aramaki, Y. Sakai, and N. Ono, Appl. Phys. Lett. **84**, 2085 (2004a).
[17] S. Aramaki, Y. Sakai, R. Yoshiyama, K. Sugiyama, N. Ono, and J. Mizuguchi, Proc. SPIE **5522**, 27 (2004).
[18] S. Aramaki and J. Mizuguchi, Acta Crystallogr. **E59**, o1556 (2003).
[19] P. B. Shea, J. Kanicki, and N. Ono, J. Appl. Phys. **98**, 014503 (2005).
[20] S. Ito, T. Murashima, H. Uno, and N. Ono, Chem. Commun. (Cambridge) **1998**, 1661.
[21] S. Ito, N. Ochi, T. Murashima, H. Uno, and N. Ono, Heterocycles **52**, 399

(2000).
[22]Y. Shimizu, Z. Shen, T. Okujima, H. Uno, and N. Ono, Chem. Commun. (Cambridge) **2004**, 374.
[23]O. S. Finikova, A. V. Cheprakov, I. P. Beletskaya, P. J. Carroll, and S. A. Vinogradov, J. Org. Chem. **69**, 522 (2004).
[24]G. E. Engel, S. Wilke, K. D. M. Harris, and F. J. J. Leusen, J. Appl. Crystallogr. **32**, 1169 (1999).
[25]R. A. Young, *The Rietveld Method*, IUCr Monographies of Crystallography 5 (Oxford University Press, Oxford, 1993).
[26]D. A. Van Veldhuizen and G. B. Lamont, Evol. Comput. **8**, 125 (2000).
[27]E. B. Fleischer, C. K. Miller, and L. E. Webb, J. Am. Chem. Soc. **86**, 2342 (1964).
[28]E. B. Fleischer, Acc. Chem. Res. **3**, 105 (1970).
[29]W. Jentzen, I. Turowska-Tyrk, W. R. Scheidt, and J. A. Shelnutt, Inorg. Chem. **35**, 3559 (1996).
[30]M. W. Renner, L. R. Furenlid, K. M. Barkigia, and J. Fajer, J. Phys. IV **7**, 661 (1997).
[31]M. S. Liao, J. D. Watts, and M. J. Huang, J. Phys. Chem. A **109**, 11996 (2005).
[32]X.-Z. Song, W. Jentzen, L. Jaquinod, R. G. Khoury, C. J. Medforth, S.-L. Jia, J.-G. Ma, K. M. Smith, and J. A. Shelnutt, Inorg. Chem. **37**, 2117 (1998).
[33]M.-S. Liao and S. Scheiner, J. Chem. Phys. **117**, 205 (2002).
[34]H.-H. Tsai and M. C. Simpson, J. Phys. Chem. A **108**, 1224 (2004).
[35]S. Cromer, P. Hambright, J. Grodkowski, and P. Neta, J. Porphyr. Phthalocyanines **1**, 45 (1997).
[36]R. A. Birnstead, M. J. Crossley, and N. S. Hush, Inorg. Chem. **30**, 1259 (1991).
[37]*The Porphyrin Handbook*, edited by K. M. Kadish, K. M. Smith, and R. Guilard (Academic, New York, 1999).
[38]X. Zhou, A. Ren, J. Feng, and X. Liu, Can. J. Phys. **82**, 19 (2004).
[39]L. Edwards, D. H. Dolphin, M. Gouterman, and A. D. Adler, J. Mol. Spectrosc. **38**, 16 (1971).
[40]C. J. Schramm, R. P. Scaringe, D. R. Stojakovic, B. M. Hoffman, J. A. Ibers, and T. J. Marks, J. Am. Chem. Soc. **102**, 6702 (1980).
[41]P. K. Bhattacharya, *Semiconductor Optoelectronic Devices*, 2nd ed. (Prentice Hall, Upper Saddle River, NJ, 1997).
[42]B. Saleh and M. Teich, *Fundamentals of Photonics*, 1st ed. (Wiley-Interscience, New York, 1991).
[43]J. Singh, *Electronic and Optoelectronic Properties of Semiconductor Structures* 1st ed. (Cambridge University Press, Cambridge, 2003).
[44]J. Kanicki and S. Martin, in *Printed Organic and Molecular Electronics*, edited by D. Gamota, P. Brazis, K. Kalyanasundaram, and J. Zhang (Kluwer Academic, Dordrecht, 2004).
[45]G. Horowitz, Adv. Mater. (Weinheim, Ger.) **10**, 365 (1998).
[46]S. Scheinert and G. Paasch, Phys. Status Solidi A **201**, 1263 (2004).
[47]H. Sirringhaus, Adv. Mater. (Weinheim, Ger.) **17**, 2411 (2005).
[48]J. Z. Wang, J. F. Chang, and H. Sirringhaus, Appl. Phys. Lett. **87**, 083503 (2005).
[49]G. Merckel and A. Rolland, Solid-State Electron. **39**, 1231 (1996).
[50]M. C. Hamilton, S. Martin, and J. Kanicki, Chem. Mater. **16**, 4699 (2004).
[51]P. Stallinga, H. Gomes, F. Biscarini, M. Murgia, and D. de Leeuw, J. Appl. Phys. **96**, 5277 (2004).
[52]A. Rolland, J. Richard, J. P. Kleider, and D. Mencaraglia, J. Electrochem. Soc. **140**, 3679 (1993).
[53]S. M. Sze, *Physics of Semiconductor Devices* (Wiley, New York, 1981).
[54]M. Kiguchi, M. Nakayama, K. Fujiwara, K. Ueno, T. Shimada, and K. Saiki, Jpn. J. Appl. Phys., Part 2 **42**, L1408 (2003).
[55]P. B. Shea, A. R. Johnson, J. Kanicki, and N. Ono, IEEE Trans. Electron Devices **52**, 1497 (2005).
[56]A. Kohno, T. Sameshima, N. Sano, M. Sekiya, and M. Hara, IEEE Trans. Electron Devices **42**, 251 (1995).
[57]M. C. Hamilton, S. Martin, and J. Kanicki, IEEE Trans. Electron Devices **51**, 877 (2004).
[58]J. Martinsen, L. J. Pace, T. E. Phillips, B. M. Hoffman, and J. A. Ibers, J. Am. Chem. Soc. **104**, 83 (1982).
[59]F. W. Kutzler and D. E. Ellis, J. Chem. Phys. **84**, 1033 (1986).